Topological quantization by controlled paths: Application to Cooper pairs pumps

Raphael Leone and Laurent Lévy
Institut Néel, CNRS–Université Joseph Fourier, Boîte Postale 166, 38042 Grenoble Cedex 9, France
(Received 29 October 2007; published 29 February 2008)

When physical systems are tunable by three classical parameters, level degeneracies may occur at isolated points in parameter space. A topological singularity in the phase of the degenerate eigenvectors exists at these points. When a path encloses such point, the accumulated geometrical phase is sensitive to its presence. Furthermore, surfaces in parameter space enclosing such point can be used to characterize the eigenvector singularities through their Chern indices, which are integers. They can be used to quantize a physical quantity of interest. This quantity changes continuously during an adiabatic evolution along a path in parameter space. Quantization requires to turn this path into a surface with a well defined Chern index. We analyze the conditions necessary to a *topological quantization by controlled paths*. It is applied to Cooper pair pumps. For more general problems, a set of four criteria is proposed to check if topological quantization is possible.

DOI: 10.1103/PhysRevB.77.064524 PACS number(s): 85.25.Cp, 03.65.Vf, 74.50.+r, 74.78.Na

I. INTRODUCTION

Using nanometer size Josephson junctions, a huge variety of superconducting quantum circuits can be made. These circuits are described by simple Hamiltonians involving a discrete set of quantum variables. They are typically the excess number of Cooper pairs $\hat{n}_j$ on superconducting elements, and their canonical conjugate variables $\hat{\Theta}_j$ ($[\hat{n}_j, \hat{\Theta}_j]=i$) are related to the quantum phases of the superconducting order parameters of the circuit islands. In addition, most circuits have tunable elements: They are control voltages on gates or, using magnetic fluxes, quenched quantum phases or Josephson couplings. These circuits are most often used to implement quantum logic,[1,2] where the quantum gates are controlled with voltage or resonant microwave pulses on some of gates or other tunable elements.

The tunable elements of quantum circuits can also be used to generate adiabatic evolutions of the Hamiltonian as a function of the parameters. More precisely, the N induced gate charges n_{gi} and control phases φ_i define a vector $\mathbf{R}=\{n_{g1}\cdots\varphi_1\cdots\}$ in the parameter space $\mathbb{P}$ of dimension N. Let $E_\alpha(\mathbf{R})\cdots$ and $|\alpha(\mathbf{R})\rangle\cdots$ be the eigenenergies (bands) and eigenvectors of the Hamiltonian $\hat{\mathcal{H}}(\mathbf{R})$. At a point $\mathbf{R}$ and for a nondegenerate band α, one can construct a fiber defined by the set of all vectors $\{|\alpha(\mathbf{R})\rangle\}$, which may differ by a complex factor. The set of all these fibers defines the fiber bundle over the parameter space $\mathbb{P}$. When the topology of this bundle becomes nontrivial, physical phenomena of great interest can occur.

Parallel transport, holonomy, and homotopy are central concepts for the physics of geometric phases. Berry's phase is one of these and is a relevant quantity when adiabaticity conditions hold for a globally nondegenerate band. In this case, Berry's phase is the geometric part of the phase acquired by the wave function along an adiabatic cycle over a closed path Γ^c in the parameter space $\mathbb{P}$.

Depending on the nature of the quantum system studied, the physical consequences of the nontrivial topology of the eigenvector bundle are different. A number of physical examples have been studied in several areas of physics. In molecular systems, the electronic structure depends on the semiclassical nuclear coordinates (within the Born-Oppenheimer approximation), which define the parameter space. Their energy manifolds can have conical intersections at isolated values of the nuclear coordinates:[3–5] These so-called "diabolical points" are directly responsible for the change of multiplicity of rotation-vibration levels as a function of nuclear coordinates. In molecular magnets, the magnetic energy levels depend on the direction and magnitude of the applied magnetic field (the parameter space) with respect to the molecular axes. For some molecules, isolated degeneracies have also been found for specific directions and values of the magnetic field.[6,7] At these points, quantum tunneling is quenched as a result of interferences caused by the wave function phase changes around the "defect." Indeed, this phase change takes a particular value of π for physically relevant paths encircling the degeneracy, leading to the destructive interferences observed.

In the few examples above, degeneracies occur at isolated conical intersections between two energy bands in a three-dimensional parameter space. These diabolical points are singularities of the quantum phase field over the parameter space and responsible for the "exotic topologies." Closed paths, through Berry's phase, are sensitive probes of the topology. Closed surfaces in a three-dimensional parameter space are also sensitive to the presence of conical points through a topological invariant called the Chern index c_1, which is an integer number. Some of the best known phenomena in condensed matter physics are well understood in terms of Chern indices, such as integer quantum Hall effect (IQHE),[8,9] Thouless pumping (TP),[10] or ac Josephson effect (ac JE).[10,11] Physical quantities that can be expressed in terms of Chern indices are subject to *topological quantization*. This is why they are used in metrology. For instance, the IQHE gives a conversion from voltage unit (volt) to current unit (ampere) through the resistance quantum $R_K=\frac{h}{e^2}$: $V=\frac{R_H}{c_1}I$; in the same way, the ac Josephson effect gives a conversion from voltage to frequency (in hertz) through the magnetic flux quantum $\Phi_0=\frac{h}{2e}$: $V=\Phi_0\nu$.

Such physics can be encountered in the simplest superconducting circuit depending on three *tunable* parameters: One is the Cooper pair pump (CPP), where degeneracies

occur at isolated points in the parameter space. Here, the parameter space is constructed from two gate voltages V_{gi} and a quenched quantum phase φ. However, an essential difference subsists between the examples given above and this problem. In the case of IQHE, TP, or ac JE, the relevant physical quantity measured is directly proportional to the Chern index of the surface brought into play (the magnetic Brillouin zone for the IQHE). In a CPP, one can only make (adiabatic) paths in the parameter space by modifying the parameters in order to tune the current delivered by the CPP. Thus, Berry's phase seems to be, *a priori*, the relevant topological quantity characterizing the paths. This will be shown to always be the case by relating the charge transferred by the CPP through a path in terms of Berry's phase, even for open paths. Nevertheless, Chern indices can also specify the value of the current for specific paths covering densely a closed surface enclosing a diabolical point. The degree of quantization of the current delivered by this method improves exponentially with the degree of the surface coverage. This form of quantization is referred to as "topological quantization by controlled paths" (TQCP). The current will be shown to be equal to $2e\nu$, where ν is a characteristic frequency of the adiabatic cycles of pumping. For metrology, the Cooper pair pumping through TQCP gives a conversion between current and frequency: It is an effect that could be used to close the metrological triangle between the units of voltage V, current I, and frequency ν.

In this paper, we emphasize what is specific to quantum circuits, and the example of the Cooper pair pump is an excellent case study for the concept of TQCP around which much of the paper is built. In Sec. II, we recall the topological properties of three-dimensional parameter spaces stressing the notions of Berry's phase and Chern indices in the presence of degeneracies. In Sec. III, the TQCP is introduced, and the computation method of the quantized physical quantity is given. In this section, the following necessary criteria for TQCP are derived.

1. The energy spectrum must be discrete (adiabaticity).

2. The Hamiltonian depends on three continuous tunable parameters, which specify the parameter space $\mathbb{P}$. Isolated *conical degeneracies* between the two lowest eigenstates $|\pm\rangle$ must occur in $\mathbb{P}$.

3. The relevant physical observable Q (the quantity measured) follows Hamilton semiclassical equation of motion $\dot{Q}=\langle\partial_\varphi\hat{\mathcal{H}}\rangle$ where the parameter φ is periodic. The contribution of this quantity along *geometrical* paths is set by the topology of the eigenvector bundle.

4. The dynamical contributions to Q must also be taken into account. The topological quantization can be implemented only when they can be eliminated. This is possible when the φ dependence of the Hamiltonian eigenvalues can be integrated out using its periodicity or other symmetries of the system.

In the Conclusion, a full discussion of these four criteria is presented in light of this work. Section V is devoted to a practical implementation of the TQCP for Cooper pair pumps. Section VI shows how microwave fields can be used to expand the parameter space to higher dimensions. In the example considered, the isolated degeneracies become a two-dimensional degenerate subspace in which non-Abelian holonomies are designed for adiabatic quantum computation.

II. TOPOLOGY OF THE PARAMETRIZED EIGENVECTOR SPACE

In this section, the topological features in parameter spaces are explained in simple words. Let a quantum system be dependent on N parameters x^μ defining a parameter space $\mathbb{P}$. Then, the Hamiltonian governing the dynamics is written as $\hat{\mathcal{H}}(\mathbf{R})$, where $\mathbf{R}=(x^1,x^2,\ldots,x^N)$ is a vector in $\mathbb{P}$. The parameters are classical and can be tuned by an observer. Modifying the parameters amounts to trace a path Γ in the parameter space, parametrized by time. To each point $\mathbf{R}$ in $\mathbb{P}$ is assigned the set $\{|\beta(\mathbf{R})\rangle\}$ of eigenstates of $\hat{\mathcal{H}}(\mathbf{R})$, with the dimensionality of the Hilbert space $\mathcal{E}$. More precisely, for a single nondegenerate level α, a *fiber* $\mathcal{F}^{(\alpha)}_{\mathbf{R}}$ attach the eigenvector $|\alpha(\mathbf{R})\rangle$ to point $\mathbf{R}$ as

$$\mathcal{F}^{(\alpha)}_{\mathbf{R}}=\{|\alpha\rangle \text{ such that } \hat{\mathcal{H}}(\mathbf{R})|\alpha\rangle=E_\alpha(\mathbf{R})|\alpha\rangle\}. \tag{1}$$

This fiber is defined everywhere in $\mathbb{P}$, except where band α is degenerate. The set of all fibers attached to $\mathbb{P}$ defines the *vector bundle* $\mathcal{F}^{(\alpha)}$ over the parameter space: For a nondegenerate band α, it is a complex line bundle. A *connection* is a differentiable rule for a shift from the fiber $\mathcal{F}^{(\alpha)}_{\mathbf{R}}$ to $\mathcal{F}^{(\alpha)}_{\mathbf{R}+d\mathbf{R}}$ when $\mathbf{R}$ moves to $\mathbf{R}+d\mathbf{R}$ in parameter space. When considering the adiabatic evolution of a quantum state $|\tilde{\alpha}(\mathbf{R})\rangle$, *parallel transport* connections are involved. They are such that $\Im m\langle\tilde{\alpha}(\mathbf{R})|d\tilde{\alpha}(\mathbf{R})\rangle=0$ everywhere along the path Γ covered. This requires that the path Γ never crosses a point where band α is degenerate. For a smooth choice of normalized states $|\alpha(\mathbf{R})\rangle$, the parallel transport condition on a state $|\tilde{\alpha}\rangle=e^{i\gamma_\alpha}|\alpha\rangle$ is equivalent to a time evolution of the phase $\dot{\gamma}_\alpha=i\langle\alpha|\dot{\alpha}\rangle$, which can be integrated along the path Γ starting from $\mathbf{R}_i$ as

$$\gamma_\alpha(t)=i\int_{\mathbf{R_i}}^{\mathbf{R(t)}}\langle\alpha(\mathbf{R})|\boldsymbol{\nabla}\alpha(\mathbf{R})\rangle\cdot d\mathbf{R}. \tag{2}$$

This phase is purely geometric, i.e., independent of a reparametrization of coordinates on the path Γ. On the other hand, it is not invariant under a local gauge change: $|\alpha\rangle\rightarrow e^{i\xi(\mathbf{R})}|\alpha\rangle$, making the phase γ_α nonintegrable and multivalued. For this reason, the gauge field and its Berry's connection are specified as

$$\mathbf{A}^{(\alpha)}(\mathbf{R})=\langle\alpha(\mathbf{R})|\boldsymbol{\nabla}\alpha(\mathbf{R})\rangle, \tag{3}$$

$$\mathcal{A}^{(\alpha)}=\langle\alpha|d\alpha\rangle=\mathbf{A}^{(\alpha)}(\mathbf{R})\cdot d\mathbf{R}. \tag{4}$$

A key feature of the phase γ_α is that it becomes a gauge invariant quantity when the paths Γ^c are closed. In this case, *Berry's phase*[12]

$$\gamma_\alpha(\Gamma^c)=\oint_{\Gamma^c}\mathcal{A}^{(\alpha)} \text{ mod}[2\pi] \tag{5}$$

is a physically observable quantity and cannot be removed by any local gauge change. It is sensitive to the topology of

the fiber bundle: It is the *holonomy*[13] of the line bundle $\mathcal{F}^{(\alpha)}$ over the path Γ^c. An important special case arises when the Hamiltonian is real for a set of paths in a subspace of $\mathbb{P}$: a continuous choice of real eigenstates $|\tilde{\alpha}(\mathbf{R})\rangle$ may be chosen over this path, which defines a parallel transport since $\Im m\langle\tilde{\alpha}|d\tilde{\alpha}\rangle=0$, leading to values of 0 or π for Berry's phase, such that $|\tilde{\alpha}(\mathbf{R_f})\rangle=\pm|\tilde{\alpha}(\mathbf{R_i})\rangle$.

Berry's phase first appeared as the geometric contribution to the phase acquired in the adiabatic cyclic evolution of a nondegenerate state in the parameter space. In the next section, the state $|\psi_\alpha(t)\rangle$ of a system initially prepared in the nondegenerate state $|\alpha(\mathbf{R_i})\rangle$ evolving adiabatically along the path Γ is shown to be approximately

$$|\psi_\alpha(t)\rangle \approx e^{-i\eta_\alpha(t)}e^{i\gamma_\alpha(t)}|\alpha[\mathbf{R}(t)]\rangle, \tag{6}$$

where $\eta_\alpha(t)=\frac{1}{\hbar}\int_0^t E_\alpha(t')dt'$ is the usual dynamical phase and $|\alpha(\mathbf{R})\rangle$ is the instantaneous eigenstate.

The gauge field $\mathbf{A}^{(\alpha)}$ defined in Eq. (4) is analogous to the vector potential of electromagnetism: In three dimensions, the gauge insensitive magnetic field $\mathbf{B}^{(\alpha)}=\boldsymbol{\nabla}\times\mathbf{A}^{(\alpha)}$ is physically relevant. To characterize the properties of the fiber bundle in a gauge independent manner, it is useful to define Berry's curvature as the differential form $\mathcal{B}^{(\alpha)}=B^{(\alpha)}_{\mu\nu}dx^\mu dx^\nu \equiv i\langle d\alpha|\wedge|d\alpha\rangle$, where $B^{(\alpha)}_{\mu\nu}=\partial_\mu A^{(\alpha)}_\nu-\partial_\nu A^{(\alpha)}_\mu$ are elements of the antisymmetric curvature tensor $B^{(\alpha)}$. Using these definitions, Stokes theorem can be used to write Berry's phase of band α over the closed path Γ^c as a surface integral

$$\gamma_\alpha(\Gamma^c)=\oint_{\Gamma^c}\mathcal{A}^{(\alpha)}=\int\int_{\mathcal{S}}\mathcal{B}^{(\alpha)}, \tag{7}$$

where $\mathcal{S}$ is an oriented surface with Γ^c as a border. Systems depending on a set of three parameters x^1, x^2, and x^3 are most pertinent for TQCP. The orientation of $\mathbb{P}$ is defined by a local choice of basis, for instance, the natural basis $(\mathbf{u}_1,\mathbf{u}_2,\mathbf{u}_3)$ with respect to the coordinates x^μ. Using ordinary vector calculus, the antisymmetric curvature tensor $B^{(\alpha)}$ reduces to a magnetic field $\mathbf{B}^{(\alpha)}$, the curl of $\mathbf{A}^{(\alpha)}$. $\mathbf{B}^{(\alpha)}$ can be computed directly from the Hamiltonian gradient as[12]

$$\mathbf{B}^{(\alpha)}=i\sum_{\beta\neq\alpha}\frac{\langle\alpha|\boldsymbol{\nabla}\hat{\mathcal{H}}|\beta\rangle\times\langle\beta|\boldsymbol{\nabla}\hat{\mathcal{H}}|\alpha\rangle}{(E_\alpha-E_\beta)^2}, \tag{8}$$

where $\{|\beta\rangle\}$ is the set of eigenstates of $\hat{\mathcal{H}}$ dependent on $\mathbf{R}$. As we shall see below, nonzero Berry's phases occur from a nontrivial topology of the eigenvectors fiber bundle. This occurs at level degeneracies in the parameter space where the magnetic field $\mathbf{B}^{(\alpha)}$ is singular. At these points, $\boldsymbol{\nabla}\cdot\mathbf{B}^{(\alpha)}\neq\mathbf{0}$ and $\mathbf{A}^{(\alpha)}$ cannot be defined. Without such points, the topology is trivial and the parallel transport leaves states invariant over a closed loop: $|\tilde{\alpha}(\mathbf{R_f})\rangle=|\tilde{\alpha}(\mathbf{R_i})\rangle$.

The von Neumann–Wigner theorem[14] asserts that in a three-dimensional parameter space, accidental degeneracies may occur between two neighboring levels (say, $|\pm\rangle$) only at isolated points $\mathbf{R}^*_\mathbf{i}$; these degeneracies which are singularities of the fields $\mathbf{B}^{(\pm)}$ have been named *normal singular points* by Simon.[13] Since the gauge fields $\mathbf{A}^{(\pm)}$ do not exist at these points, they become local quantities. Interesting physics appear when such points live in $\mathbb{P}$. It can be visualized most easily by projecting the Hamiltonian on the two-level manifold $|\pm\rangle$, which becomes degenerate at the singular point $\mathbf{R}^*=(x^1_*,x^2_*,x^3_*)$. Using the projector $\hat{P}=|+\rangle\langle+|+|-\rangle\langle-|$, a gradient expansion of the two-level projection $\hat{\mathcal{H}}_\pm$ of the Hamiltonian can be made in the vicinity of the singularity $\mathbf{R}^*$,

$$\hat{P}[\hat{\mathcal{H}}(\mathbf{R})-\hat{\mathcal{H}}(\mathbf{R}^*)]\hat{P}=\hat{\mathcal{H}}_\pm(\mathbf{R})-\hat{\mathcal{H}}_\pm(\mathbf{R}^*)$$
$$=\boldsymbol{\nabla}\hat{\mathcal{H}}_\pm(\mathbf{R}^*)\cdot\delta\mathbf{R}+O(\delta\mathbf{R}^2), \tag{9}$$

where $\delta\mathbf{R}=\mathbf{R}-\mathbf{R}^*=(\delta x^1,\delta x^2,\delta x^3)$. With a suitable choice for the origin of energies $[E_\pm(\mathbf{R}^*)=0]$, $\hat{\mathcal{H}}_\pm(\mathbf{R}^*)$ is zero. With this choice, this expansion can be expressed on the basis of Pauli matrices as

$$\hat{\mathcal{H}}_\pm(\mathbf{R})=\frac{1}{2}\sum_{\mu,\nu=1}^{3}c^\nu_\mu\delta x^\mu\sigma_\nu. \tag{10}$$

The c^ν_μ are the elements of a 3×3 real matrix $\hat{C}$, which has a nonzero determinant for linear level crossing at $\mathbf{R}^*$. This becomes more familiar by defining $\mathbf{b}=\hat{C}\delta\mathbf{R}=(b^x,b^y,b^z)$ as the effective magnetic field for an equivalent spin-$\frac{1}{2}$ spin system,

$$\hat{\mathcal{H}}_\pm(\mathbf{R})=\frac{1}{2}\boldsymbol{\sigma}\cdot\mathbf{b}(\mathbf{R})=\frac{1}{2}\begin{pmatrix}b^z & b^x-ib^y\\ b^x+ib^y & -b^z\end{pmatrix}, \tag{11}$$

whose magnitude increases linearly with the deviation from the degeneracy point $\mathbf{b}^*=\mathbf{0}$. The energy levels $E_\pm=\pm\frac{|\mathbf{b}|}{2}$ of the two bands intersect conically at the degeneracy point (also called *conical point* or diabolical point). The matrix $\hat{C}$ maps a local neighborhood of $\mathbf{R}^*$ of the parameter space onto a spatially isotropic spin-$\frac{1}{2}$ Hamiltonian in the magnetic field $\mathbf{b}$. As long as the mapping amounts to a local deformation of the parameter space, and no additional degeneracies appear in the vicinity of $\mathbf{R}^*$, the topology of the fiber bundle stays unchanged. If $\hat{C}$ changes the orientation of space [the det $(\hat{C})$ is negative], the sign of the topological charge is flipped by the mapping. The one-to-one mapping $\hat{C}$ allows us to use the Euler angles of $\mathbf{b}$ rather than the coordinate $\delta\mathbf{R}$ to specify the eigenstates in the vicinity of the singularity as

$$|+(\mathbf{b})\rangle=\begin{pmatrix}\cos\frac{\theta}{2}\\ e^{i\phi}\sin\frac{\theta}{2}\end{pmatrix},\quad |-(\mathbf{b})\rangle=\begin{pmatrix}-\sin\frac{\theta}{2}\\ e^{i\phi}\cos\frac{\theta}{2}\end{pmatrix}. \tag{12}$$

For both levels, one can assign Berry's gauge potentials $\mathbf{A}^{(\pm)}$,

$$\mathbf{A}^{(\pm)}=i\langle\pm|\boldsymbol{\nabla}_\mathbf{b}\pm\rangle=\pm\frac{\cos\theta\mp1}{2|\mathbf{b}|\sin\theta}\mathbf{e}_\phi. \tag{13}$$

These are the azimuthal gauge fields of "Dirac monopoles" of strength $+\frac{1}{2}$ or $-\frac{1}{2}$ placed at the origin. They are singular on their *Dirac string* ($\theta=\pi$ for $|+\rangle$ and $\theta=0$ for $|-\rangle$). These

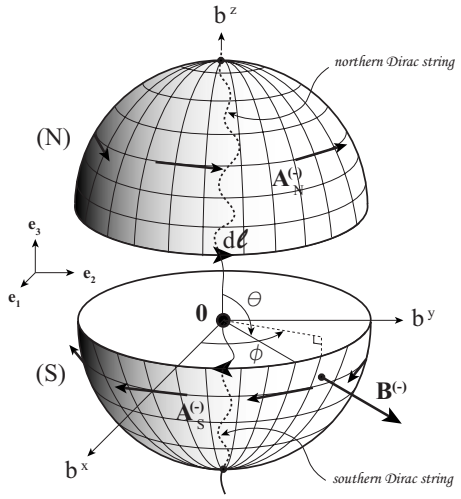

FIG. 1. A monopole placed at the degeneracy points generates azimuthal vector potentials $\mathbf{A}^{(\pm)}$ for each quantum band $|\pm\rangle$ intersecting at the monopole. Because of the singularity, a single valued expression for $\mathbf{A}^{(\pm)}$ exists separately in the upper and lower half hemispheres. They can be connected on the equator by a clutching function ($\mathbf{A}^{(-)}$ is pictured here). The corresponding magnetic fields $\mathbf{B}^{(\pm)}$ are radial and decrease as b^{-2}, where b is the distance to the singularity.

monopoles produce a radial magnetic field of opposite directions,

$$\mathbf{B}^{(\pm)} = \boldsymbol{\nabla}_{\mathbf{b}} \times \mathbf{A}^{(\pm)} = \mp \frac{\mathbf{b}}{2|\mathbf{b}|^3}. \tag{14}$$

The strengths $\pm\frac{1}{2}$ are more easily identified by taking the divergence

$$\boldsymbol{\nabla}_{\mathbf{b}} \cdot \mathbf{B}^{(\pm)} = \mp \frac{1}{2}\delta(\mathbf{b}), \tag{15}$$

which, integrated over any volume including the origin, gives $\pm\frac{1}{2}4\pi$. Since the one-to-one mapping $\hat{C}$ between parameter space and spin space conserves the flux, the topological charge in $\mathbb{P}$ is preserved up to a sign (when $\hat{C}$ changes the surface orientations).

The degeneracies ($\mathbf{R}_\mathbf{i}^*$) in parameter space appear as singularities of the fields $\mathbf{A}^{(\pm)}$. Since any surface $\mathcal{S}$ enclosing $\mathbf{R}^*$ intersects the Dirac string, $\mathbf{A}^{(\pm)}$ is not defined everywhere on $\mathcal{S}$. It is possible to make $\mathbf{A}^{(\pm)}$ single valued only by making a hole in $\mathcal{S}$ through which the Dirac string can be threaded: In this case, the surface can be continuously contracted to a point without crossing the singularity $\mathbf{R}^*$. This is the reason why there is no single analytic expression of $\mathbf{A}^{(\pm)}$ over a surface which encloses completely the degeneracy. An alternative procedure for defining $\mathbf{A}^{(\pm)}$ was made by Wu and Yang.[15] The space is divided in north (N) and south (S) halves (see Fig. 1), with a different gauge choice $\mathbf{A}^{(\pm)}$ in each part, which are related by an appropriate *clutching function* $f^{(\pm)}$ on the equator where the eigenstates are connected using $|\pm\rangle_N = e^{if^{(\pm)}}|\pm\rangle_S$, with $\mathbf{A}_N^{(\pm)} = \mathbf{A}_S^{(\pm)} + \boldsymbol{\nabla} f^{(\pm)}$. For the isotropic spin-$\frac{1}{2}$ model, the different determinations of $\mathbf{A}^{(\pm)}$ are

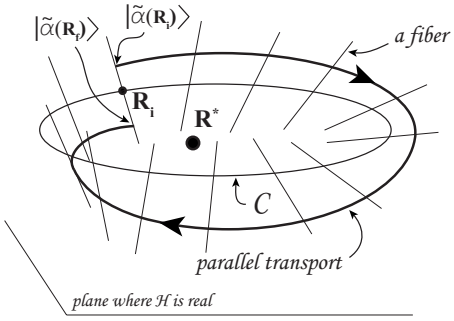

FIG. 2. Illustration of a circular path $\mathcal{C}$ around a degeneracy, lying in a plane where the Hamiltonian is real. The real eigenstates depend on a single angle variable. This angle specifies the direction of a line. Under a parallel transport along loop, this line (the eigenvector) generates a Mœbius strip, which is the visual representation of the eigenvector bundle. The eigenstate changes sign when coming back to the same point. This sign is the holonomy of the eigenstate fiber.

$$\mathbf{A}^{(\pm)} = \pm \begin{cases} \dfrac{\cos\theta - 1}{2|\mathbf{b}|\sin\theta} = \mathbf{A}_N^{(\pm)} & \text{for } \theta \in \left[0; \dfrac{\pi}{2}\right) \\ \dfrac{\cos\theta + 1}{2|\mathbf{b}|\sin\theta} = \mathbf{A}_S^{(\pm)} & \text{for } \theta \in \left(\dfrac{\pi}{2}; \pi\right], \end{cases} \tag{16}$$

with $f^{(\pm)} = \mp\phi$ as the clutching function.

On a closed path Γ^c, Berry's phase for the two levels $\pm$ is sensitive to the presence of a degeneracy at the origin since

$$\gamma_\pm(\Gamma^c) = \oint_{\Gamma^c} \mathbf{A}^{(\pm)} \cdot d\ell = \mp \frac{1}{2}\Omega(\Gamma^c), \tag{17}$$

where $\Omega(\Gamma^c)$ is the solid angle seen from the origin. When Γ^c is contained in a plane intersecting the origin, then $\gamma_\pm(\Gamma^c)$ is just equal to π times the winding number of Γ^c around the origin. This discussion makes it clear that it is a consequence of the nontrivial topology of the bundles $\mathcal{F}^{(\pm)}$ around the origin. A geometrical illustration is possible when path $\mathcal{C}$ shown in Fig. 2 lies in a plane where the Hamiltonian is real: The spin eigenstates $|\pm\rangle$, which can be taken as real, depends on a single angle variable (say, θ) that defines a line. As one moves along Γ^c, this line, which represents the eigenvector bundle, covers a one-twist Mœbius strip, as illustrated in Fig. 2. In this parallel transport, initial and final states are seen to be opposite $|\pm(\mathbf{b_f})\rangle = -|\pm(\mathbf{b_i})\rangle$: Berry's phase equals π. It is also the well-known property of the group SU(2), where rotations are 4π periodic. In general, if the path encircles m degeneracies and has a winding number n_i around the degeneracy at points $\mathbf{R}_i^*$, Berry's phase is $0 \bmod [2\pi]$ if $\Sigma_{i=1}^m n_i$ is even and π otherwise.

Berry's phase factors for loops in planes where the Hamiltonian is real are *topological invariants* ± 1, which characterize the sum of winding numbers around degeneracies. Another topological invariant is obtained after integrating the field $\mathbf{B}^{(\pm)}$ of Eq. (14) over a small sphere $\mathbb{S}^2$ around the origin. When normalized to 2π, these flux gives the first Chern numbers (or *Chern indices*) of the sphere with respect to the two bands $|\pm\rangle$:

$$c_1^{(\pm)}(\mathbb{S}^2) = \frac{1}{2\pi}\oiint_{S^2} \mathbf{B}^{(\pm)} \cdot \hat{n} dS = \mp 1, \tag{18}$$

where $\hat{n}$ is the unit vector normal to the surface of the sphere. The Chern index can also be computed from the potentials $\mathbf{A}^{(\pm)}$ using

$$\begin{aligned} c_1^{(\pm)}(\mathbb{S}^2) &= \frac{1}{2\pi}\oint_{\mathcal{C}} (\mathbf{A}_N^{(\pm)} - \mathbf{A}_S^{(\pm)}) \cdot d\ell \\ &= \frac{1}{2\pi}\oint_{\mathcal{C}} \boldsymbol{\nabla}_{\mathbf{b}} f^{(\pm)} \cdot d\ell \\ &= \mp \frac{1}{2\pi}\int_0^{2\pi} d\phi = \mp \frac{1}{2\pi}(2\pi - 0) = \mp 1. \end{aligned} \tag{19}$$

The mapping $\hat{C}$ between the parameter space $\mathbb{P}$ and the isotropic space $\mathbb{R}^3$ does not change Chern indices if space orientation is preserved $[\det(\hat{C}) > 0]$.

Topological indices do not depend on the projection on a two-level system, which is valid only in a small neighborhood of $\mathbf{R}^*$. For any band α and any closed surface $\mathcal{S}$ in $\mathbb{P}$, Gauss theorem assures that the integral of $\mathbf{B}^{(\alpha)}$ over the entire surface is identical to the sum of the integrals over a small sphere about each degeneracy. In other words,

$$c_1^{(\alpha)}(\mathcal{S}) = \sum_{d_i \in V(\mathcal{S})} q_i^{(\alpha)}, \tag{20}$$

where $q_i^{(\alpha)}$ represents the topological charge of each degeneracy $\mathbf{R}_i^*$ inside the volume $V(\mathcal{S})$. The Chern index does not depend on the geometry of the closed surface and is a topological invariant, which depends only on the degeneracies it contains.

III. TOPOLOGICAL QUANTIZATION BY CONTROLLED PATHS

Suppose that a quantum system depends on three *tunable* parameters x^1, x^2, and x^3, which specify the space $\mathbb{P}$. One can always construct two angles $\vartheta^1(\mathbf{R})$ and $\vartheta^2(\mathbf{R}) \in [0, 2\pi)$ in $\mathbb{P}$, which parametrize a two-dimensional torus $\mathbb{T}^2$; $\boldsymbol{\vartheta} = (\vartheta^1, \vartheta^2)$ is a vector on $\mathbb{T}^2$. Q is a physical quantity that can be expressed as the partial derivative of the Hamiltonian $\hat{\mathcal{H}}(\boldsymbol{\vartheta})$ with respect to one of the angles (say, ϑ^2),

$$\dot{Q} = \langle \partial_2 \hat{\mathcal{H}}(\boldsymbol{\vartheta}) \rangle = \langle \psi | \partial_2 \hat{\mathcal{H}}(\boldsymbol{\vartheta}) | \psi \rangle. \tag{21}$$

TQCP can only be used for such physical observable, which is followed adiabatically on a path Γ_0 lying on the torus. Physically, it is the ground state expectation value of Q which is of interest. On the path Γ_0, there will be one or more avoided level crossings with other levels, and Zener tunneling in their vicinity sets the rates of variation for the parameters required for adiabaticity. Using the spin representation [Eq. (11)] close to a level crossing, where $b_z(t)$ is the tuning parameter, the condition for adiabaticity[16] may be written as

$$\hbar \dot{b}_z(t) \leqslant \frac{\pi}{2} |\mathbf{b}_\perp|^2, \tag{22}$$

with a Landau-Zener transition probability $P_{\mathrm{LZ}} = \exp\left(-\frac{\pi}{2}\frac{|\mathbf{b}_\perp|^2}{\hbar \dot{b}_z(t)}\right)$. When this condition is verified for all avoided level crossings on path Γ_0, the adiabatic theorem[17] may be applied to the nondegenerate state α whose time evolution is approximatively

$$|\psi_\alpha(t)\rangle \approx e^{-i\eta_\alpha(t) + i\gamma_\alpha(t)} |\alpha[\boldsymbol{\vartheta}(t)]\rangle, \tag{23}$$

where $|\alpha[\boldsymbol{\vartheta}(t)]\rangle$ is an instantaneous eigenstate $(\hat{\mathcal{H}}|\alpha\rangle = E_\alpha|\alpha\rangle)$, the phase $\eta_\alpha(t)$ is the usual dynamical phase factor

$$\eta_\alpha(t) = \frac{1}{\hbar}\int_0^t E_\alpha(t')dt', \tag{24}$$

and $\gamma_\alpha(t)$, Berry's geometrical phase, was introduced in the last section. In realistic systems, relaxation processes restrict the use of TQCP to the ground state, and inelastic transitions to the first excited state will be shown to dominate quantization errors.

Let us introduce the family of paths $\{\Gamma_\lambda\}$ on $\mathbb{T}^2$ differing from Γ_0 by a shift of ϑ^2 by a constant angle $\lambda \in [0, 2\pi)$. In the next sections, the helical family

$$\Gamma_\lambda : t \in [0;T] \rightarrow \boldsymbol{\vartheta}_\lambda(t) = (2\pi\nu_1 t, 2\pi\nu_2 t + \lambda), \tag{25}$$

where the angles ϑ^1 and ϑ^2 rotate at frequencies ν_1 and ν_2, will be used in a practical implementation of TQCP. When the frequencies are commensurate, the paths $\{\Gamma_\lambda\}$ are closed. One of them is represented pictorially in Fig. 4 , having commensurate frequencies $\nu_1 = 5\nu_2$. Each path Γ_λ begins at the point $\boldsymbol{\vartheta}_i = (0, \lambda)$, and the whole family $\{\Gamma_\lambda\}$ covers entirely the torus as λ is swept from 0 to 2π.

The quantity of interest is the value of "the transferred charge" $Q(\Gamma_\lambda)$ accumulated over the path $\{\Gamma_\lambda\}$, which is covered in a period T. Integrating $\dot{Q}$ over time gives

$$Q(t) = \int_0^t \langle \partial_2 \hat{\mathcal{H}}[\boldsymbol{\vartheta}(t')] \rangle dt'. \tag{26}$$

The integrand in Eq. (26) is split in two parts,

$$\partial_2 \langle \hat{\mathcal{H}} \rangle - 2\Re e \langle \psi_\alpha | \hat{\mathcal{H}} | \partial_\varphi \psi_\alpha \rangle. \tag{27}$$

Each term contributes to the transferred charge $Q(t)$: The first one leads to a dynamical contribution Q^{dyn}, while the second one specifies the geometrical pumped charge Q^{geo}. To identify the dynamical contribution, we take the time derivative of the adiabatic evolution [Eq. (23)] and apply the Schrödinger equation $i\hbar|\dot{\psi}_\alpha\rangle = \hat{\mathcal{H}}|\psi_\alpha\rangle$ to express

$$\hat{\mathcal{H}}|\psi_\alpha\rangle = e^{-i(\eta_\alpha - \gamma_\alpha)}[i\hbar|\dot{\alpha}\rangle + (E_\alpha - \hbar\dot{\gamma}_\alpha)|\alpha\rangle]. \tag{28}$$

The expectation value of $\mathcal{H}$ and its phase derivative follow from Eqs. (28) and (23),

$$\partial_2 \langle \hat{\mathcal{H}} \rangle = \partial_2 E_\alpha + \hbar \partial_2 (i\langle \alpha | \dot{\alpha} \rangle - \dot{\gamma}_\alpha). \tag{29}$$

Since $\dot{\gamma}_\alpha = i\langle \alpha | \dot{\alpha} \rangle$, the last two terms on the right hand side disappear. When integrated over period T, this first contribu-

tion $Q^{\mathrm{dyn}}(\Gamma_\lambda)$ to the transferred charge is also the derivative of the *dynamical phase* with respect to the initial angle λ,

$$Q^{\mathrm{dyn}}(\Gamma_\lambda) = \int_0^T \partial_2 E_\alpha[\boldsymbol{\vartheta}_\lambda(t)]dt = \hbar \frac{d\eta_\alpha(\Gamma_\lambda)}{d\lambda}, \tag{30}$$

where the definition [Eq. (25)] of the helical paths has been used to transform the partial derivative of the integrand into a total derivative of the dynamical phase with respect to the initial angle λ. This quantity is just the difference between the total accumulated dynamical phases on the neighboring paths $\Gamma_{\lambda+d\lambda}$ and Γ_λ normalized to the angle increment $d\lambda$.

We now turn to the geometrical contribution Q^{geo}, which comes from the second term in Eq. (27). Taking the ϑ^2 derivative of Eq. (23) yields

$$|\partial_2 \psi_\alpha\rangle = e^{-i(\eta_\alpha - \gamma_\alpha)}[|\partial_2 \alpha\rangle + i\partial_2(\gamma_\alpha - \eta_\alpha)|\alpha\rangle]. \tag{31}$$

Using Eqs. (29) and (31), the scalar product $\langle \psi_\alpha|\hat{\mathcal{H}}|\partial_2\psi_\alpha\rangle$ gives several terms, but only one of them is not purely imaginary, namely, $-i\hbar\langle\dot{\alpha}|\partial_2\alpha\rangle$. When integrated over time, the result does not depend on the dynamics, but only on the path geometry. Hence, the geometric pumped charge $Q_\alpha^{\mathrm{geo}}(\Gamma_\lambda)$ is

$$Q^{\mathrm{geo}}(\Gamma_\lambda) = -2\Re\int_0^T \langle\psi_\alpha(t)|\hat{\mathcal{H}}[\boldsymbol{\vartheta}_\lambda(t)]|\partial_2\psi_\alpha(t)\rangle dt$$

$$= \hbar\int_{\Gamma_\lambda} 2\Im\langle\partial_2\alpha[\boldsymbol{\vartheta}(t)]|d\alpha[\boldsymbol{\vartheta}(t)]\rangle. \tag{32}$$

This charge can be expressed in terms of a geometrical phase by rewriting

$$2\Im m\langle\partial_2\alpha|d\alpha\rangle = i[d\langle\alpha|\partial_2\alpha\rangle - \partial_2\langle\alpha|d\alpha\rangle]. \tag{33}$$

The second term is recognized as the ϑ^2 derivative of the connection $\mathcal{A}_\alpha$ [defined in Eq. (4)] whose integral over a closed path is Berry's phase. When integrating over the path Γ_λ, the first term only contributes at the end points $\boldsymbol{\vartheta}_i = \boldsymbol{\vartheta}_\lambda(0)$ and $\boldsymbol{\vartheta}_f = \boldsymbol{\vartheta}_\lambda(T)$, giving

$$Q^{\mathrm{geo}}(\Gamma_\lambda) = -\hbar\int_{\Gamma_\lambda}\partial_2\mathcal{A}^{(\alpha)} + i\hbar[\langle\alpha(\boldsymbol{\vartheta}_f)|\partial_2\alpha(\boldsymbol{\vartheta}_f)\rangle$$

$$-\langle\alpha(\boldsymbol{\vartheta}_i)|\partial_2\alpha(\boldsymbol{\vartheta}_i)\rangle], \tag{34}$$

these last two contributions being essential to enforce the gauge invariance of $Q^{\mathrm{geo}}(\Gamma_\lambda)$, a measurable quantity. When the path $\Gamma_\lambda^{\mathrm{c}}$ is closed, the end point contributions cancel, and $Q^{\mathrm{geo}}(\Gamma_\lambda)$ is the integral of the ϑ^2 derivative of the vector potential,[18,19]

$$Q^{\mathrm{geo}}(\Gamma_\lambda^{\mathrm{c}}) = -\hbar\oint_{\Gamma_\lambda}\partial_2\mathcal{A}^{(\alpha)}. \tag{35}$$

For the helical path family $\{\Gamma_\lambda\}$, we showed in Eq. (30) how the dynamical transferred charge $Q^{\mathrm{dyn}}(\Gamma_\lambda)$ could be expressed as the total derivative of the dynamical phase with respect to the initial angle λ. The same argument can be used here *mutatis mutandis* to the geometrical transferred charge

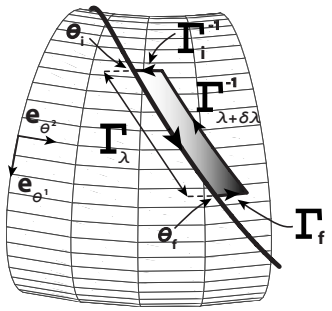

FIG. 3. The virtual path Σ_λ is the sum of the four path segments Γ_λ, Γ_f, $\Gamma_{\lambda+\delta\lambda}^{-1}$, and Γ_i^{-1} lying on the torus $\mathbb{T}^2$. The geometrical contribution Q^{geo} to the charge Q over the segment Γ_λ is proportional to the circulation of $\mathbf{A}^{(\alpha)}$ along the "virtual" closed path Σ_λ.

$$Q^{\mathrm{geo}}(\Gamma_\lambda^{\mathrm{c}}) = -\hbar\frac{d}{d\lambda}\oint_{\Gamma_\lambda^{\mathrm{c}}}\mathcal{A}^{(\alpha)} = -\hbar\frac{d\gamma_\alpha(\Gamma_\lambda^{\mathrm{c}})}{d\lambda}. \tag{36}$$

This formula presents the advantage to be easily *generalized to open paths*, thanks to the end point contributions in Eq. (34). In a first step, the integral of the angle derivative,

$$-\hbar\int_{\Gamma_\lambda}\partial_2\mathcal{A}^{(\alpha)} = \frac{\hbar}{\delta\lambda}\left[\int_{\Gamma_\lambda} + \int_{\Gamma_{\lambda+\delta\lambda}^{-1}}\right]\mathcal{A}^{(\alpha)}, \tag{37}$$

is rewritten as a difference between two paths shifted by the infinitesimal $\delta\lambda$, which becomes a sum when one of the segments is integrated in the opposite direction ($\Gamma_{\lambda+\delta\lambda}^{-1}$). These two paths can be connected by infinitesimal vertical segments Γ_i^{-1} and Γ_f at their end points $\boldsymbol{\vartheta}_i$ and $\boldsymbol{\vartheta}_f$, as shown in Fig. 3. The end point contributions in Eq. (34) can be rewritten as a line integral of the vector potential over these end segments as

$$i\hbar\langle\alpha(\boldsymbol{\vartheta}_f)|\partial_2\alpha(\boldsymbol{\vartheta}_f)\rangle = \frac{\hbar}{\delta\lambda}\int_{\Gamma_f}\mathcal{A}^{(\alpha)}$$

$$-i\hbar\langle\alpha(\boldsymbol{\vartheta}_i)|\partial_2\alpha(\boldsymbol{\vartheta}_i)\rangle = \frac{\hbar}{\delta\lambda}\int_{\Gamma_i^{-1}}\mathcal{A}^{(\alpha)}. \tag{38}$$

When combining the four path segments together, a closed path Σ_λ is constructed from the path Γ_λ, which is one of its line segments, as drawn in Fig. 3. On this closed path Σ_λ, the integral of the vector potential becomes precisely Berry's phase. By constructing the four segments' *virtual path* Σ_λ, one of which is the physical path Γ_λ of interest, the geometrical transferred charge on Γ_λ can be written as

$$Q^{\mathrm{geo}}(\Gamma_\lambda) = \hbar\frac{\gamma_\alpha(\Sigma_\lambda)}{\delta\lambda}. \tag{39}$$

In contrast with Eq. (36), which gives only a global description of the geometric charge on a closed path, this expression for the pumped charge can be used on any arbitrary paths. They are relevant if noise or error in the control of parameters exist.

What is the benefit of this formulation in terms of Berry's phase? One is practical: Berry's phase can be computed ef-

ficiently. The gauge dependence of the vector potential $\mathbf{A}^{(\alpha)}$ introduces a difficulty that can be circumvented in two ways. Berry's phase can be computed as the flux of the magnetic induction $\mathbf{B}^{(\alpha)}$ using Eq. (7). The two-dimensional integration can, however, be tedious to compute, particularly when the surface is warped. Alternatively, King-Smith and Vanderbilt[20] and Resta[21] formulated Berry's phase in terms of a gauge invariant expression by discretizing the one-dimensional path Γ_λ. Let $\boldsymbol{\vartheta}_j$ be N points on Σ_λ splitting it in N small segments. The line integral of the vector potential can then be expressed as the invariant[22]

$$\gamma_\alpha(\Sigma_\lambda) \approx -\arg \prod_{j=0}^{N-1} \langle \alpha(\boldsymbol{\vartheta}_j)|\alpha(\boldsymbol{\vartheta}_{j+1})\rangle. \tag{40}$$

In this way, any local gauge change cancels out between bras and kets, which each come in pairs. It is easy to implement over complex paths and is very accurate. When shrinking the path Γ_λ to an infinitesimal segment between $\boldsymbol{\vartheta}_\lambda(t)$ and $\boldsymbol{\vartheta}_\lambda(t+dt)$, one also gets the instantaneous geometrical pumped charge,

$$\delta Q^{\text{geo}}(t) \approx -\frac{\hbar}{\delta\lambda} \arg \prod_{j=0}^{3} \langle \alpha(\boldsymbol{\vartheta}_j)|\alpha(\boldsymbol{\vartheta}_{j+1})\rangle, \tag{41}$$

where the four points are the extremities of the infinitesimal paths (see Fig. 3). The geometrical pumped charge Q, which is a physical quantity, can be tracked and measured anywhere along any real path. Equations (39) and (41) are thus of great practical value since the local physical processes and experimental sources of errors in the path can be analyzed on the quantity of interest Q^{geo}.

For particular sets of paths (the "controlled paths"), the charge $\dot{Q}=\langle \partial_2 \hat{\mathcal{H}}\rangle$ can be quantized through its relation to the Chern index of a closed surface for the ground state eigenvector bundle. Any closed surface containing one or more singularities can, in principle, be used. For simplicity, the entire torus $\mathbb{T}^2$ will be used here. There are several ways one can generate this two-dimensional surface using a one-dimensional path. The helical family $\{\Gamma_\lambda\}$ is one of the possible families of controlled paths, which generates the surface $\mathbb{T}^2$. When the angular frequencies of ϑ^1 and ϑ^2 are commensurate $\nu_2=p\nu_1$, the angle ϑ^1 winds p times around in a ϑ^2 period. When p is large, the helix covers densely the torus. Alternatively, the initial angle λ can be swept from 0 to 2π to sweep the helix on the torus surface p times. Using this averaging procedure, the dynamical contribution to the pumped charge averages out to zero,

$$\langle Q^{\text{dyn}}\rangle = \frac{\hbar}{2\pi}\int_0^{2\pi} \frac{d\eta_\alpha(\Gamma_\lambda^c)}{d\lambda} d\lambda = \hbar(\eta_\alpha(\Gamma_{2\pi}^c) - \eta_\alpha(\Gamma_0^c)) = 0, \tag{42}$$

since $\Gamma_{2\pi}^c \equiv \Gamma_0^c$. When discussing the geometrical contribution $\langle Q^{\text{geo}}\rangle$, it is simpler to split the helix into p one-turn segments $\Gamma_\lambda^{1\ \text{turn}}$ (which are open paths). As the initial angle λ of the helix is swept from 0 to 2π, each one-turn segment $\Gamma_\lambda^{1\ \text{turn}}$ sweeps the torus surface just once (p times for the whole helix). For this reason, it is simplest to compute the

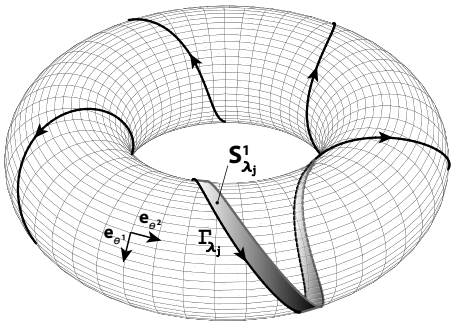

FIG. 4. Representation of a closed helical path $\Gamma_{\lambda_j}^c$ lying on the torus $\mathbb{T}^2$ (here with a frequency ratio $\nu_2/\nu_1=5$). The geometrical contribution Q^{geo} of the charge Q over a period $T_2=\frac{2\pi}{\nu_2}$ is proportional to the flux of $\mathbf{B}^{(\alpha)}$ through the infinitesimally thin strip $\mathbf{S}^1_{\lambda_j}$.

average of the geometric charge over a 2π λ period for this one-turn segment $\Gamma_\lambda^{1\ \text{turn}}$ and multiply the result by p for the whole helix. The integral over λ can be made by dividing the 2π period in N small slices indexed by j of width $\Delta\lambda=\frac{2\pi}{N}$.

The contribution to the pumped charge over the one-turn segment $\Gamma_{\lambda_j}^{1\ \text{turn}}$ for the jth slice of width $\Delta\lambda$ defines the helix strip of surface $S_{\lambda_j}^1$ represented in Fig. 4. Its boundary is nothing but the virtual path $\Sigma_j^{1\ \text{turn}}$ associated with the one-turn segment $\Gamma_{\lambda_j}^{1\ \text{turn}}$ (see Fig. 3). Using Eq. (39), the pumped charge averaged over this interval is

$$\Delta Q_\alpha^{\text{geo}}(\Gamma_{\lambda_j}^{1\ \text{turn}}) = \frac{\hbar}{\Delta\lambda}\gamma_\alpha(\Sigma_j^{1\ \text{turn}}) = \frac{\hbar}{\Delta\lambda}\oint_{\Sigma_j^{1\ \text{turn}}} \mathbf{A}^{(\alpha)}\cdot d\mathbf{R}$$

$$= \frac{\hbar}{\Delta\lambda}\int\int_{S_{\lambda_j}^1} \mathbf{B}^{(\alpha)}\cdot \hat{n}d\mathcal{S}, \tag{43}$$

where the Stokes theorem was used to express Berry's phase along the virtual path $\Sigma_\lambda^{1\ \text{turn}}$ as the flux of $\mathbf{B}^{(\alpha)}$ through $S_{\lambda_j}^1$. When summing over all the j slices of height $\Delta\lambda$, these elementary surfaces add up to the entire surface of the torus. Hence, when averaged over λ, the geometrical charge transferred becomes

$$\langle Q_\alpha^{\text{geo}}\rangle = \lim_{N\to\infty}\frac{1}{N}\sum_{j=1}^{N} Q_\alpha^{\text{geo}}(\Gamma_{\lambda_j}^{1\ \text{turn}}) = \frac{\hbar}{2\pi}\sum_{j=1}^{N}\gamma_\alpha(\Sigma_{\lambda_j})$$

$$= \frac{\hbar}{2\pi}\oiint_{\mathbb{T}^2}\mathbf{B}^{(\alpha)}\cdot\hat{n}d\mathcal{S}. \tag{44}$$

This last term is precisely the Chern index $c_1^{(\alpha)}$ of the surface $\mathbb{T}^2$ for the α-eigenvector bundle. For the whole helix, each one-turn segment contributes equally and

$$\langle Q^{\text{geo}}\rangle = p\hbar c_1^{(\alpha)}(\mathbb{T}^2). \tag{45}$$

The average of Q^{geo} over the family $\{\Gamma_\lambda^c\}$ is quantized by the winding number p, and the Chern index of the torus $\mathbb{T}^2$ with respect to band α. It is nonzero only if degeneracies involving band α are present inside the torus. As was pointed out by Goryo and Kohmoto,[11] invariances of the Hamiltonian under mirror symmetries $(\vartheta_1,\vartheta_2)\to\{(-\vartheta_1,\vartheta_2)$ or $(\vartheta_1,$

$-\vartheta_2)\}$ [i.e., $\hat{\mathcal{H}}(\vartheta_1,\vartheta_2)=\hat{\mathcal{H}}(-\vartheta_1,\vartheta_2)$ or $\hat{\mathcal{H}}(\vartheta_1,-\vartheta_2)$] and "time-reversal" symmetry $\boldsymbol{\vartheta}\to-\boldsymbol{\vartheta}$ [i.e., $\hat{\mathcal{H}}(\boldsymbol{\vartheta})=\hat{\mathcal{H}}^*(-\boldsymbol{\vartheta})$] are incompatible with a nonzero Chern index. This is because $\mathbf{B}^{(\alpha)}$ is an axial vector: The mirror symmetry $(\vartheta_1,\vartheta_2)\to(\vartheta_1,-\vartheta_2)$ leaves the torus invariant, but $\mathbf{B}^{(\alpha)}$ changes sign with respect to the local natural basis $(\mathbf{e}_{\vartheta^1},\mathbf{e}_{\vartheta^2},\hat{n})$ ($\hat{n}$ is the vector normal to the surface). Hence, the mirror symmetry switches the sign of $\mathbf{B}^{(\alpha)}(\vartheta^1,\vartheta^2)\cdot\hat{n}$, and the integral of $\mathbf{B}^{(\alpha)}\cdot\hat{n}$ over the torus vanishes. This property can be used locally to detect the presence of singularities in the eigenvector bundle. For example, in the spin representation [Eq. (11)] close to a singularity, under the mirror symmetry $(b_z\to-b_z)$, $|+\rangle$ and $|-\rangle$ are mapped into each other and each eigenvector bundle is not preserved separately. The same behavior occurs under time reversal.

Goryo and Kohmoto[11] generalized the relation between the expectation value of a derivative of the Hamiltonian and the Chern indices on D-dimensional tori, with application to a number of problems (IQHE in two and three dimensions, ac JE, etc.). In these problems, the averaging over the whole torus can be made directly, but in our case the physical quantity Q is generated by paths: A path description cannot be avoided. Since the average $\langle Q\rangle$ over a family of commensurate paths $\{\Gamma_\lambda^c\}$ is quantized, the value of $Q(\Gamma_\lambda^c)$ for a given λ fluctuates around the integer mean value. It is interesting to know how these fluctuations decrease with winding number. Since the torus is covered densely at large p, we expect a more accurate quantization as the winding number p get larger, irrespective of the value of λ. A more accurate averaging of the dynamical charge improves the quantization. This will be easiest if ϑ^2 dependence of the energy $E_\alpha(\vartheta^2)$ is weak since $Q^{\mathrm{dyn}}\sim\partial_2 E_\alpha$. TQCP is an asymptotic quantization, which works best for the ground state, which is most robust against incoherent processes. For a two-dimensional torus, a number of paths can be chosen, the only requirement for TQCP being the ϑ^2 periodicity.

The next section, devoted to the Cooper pair pump, is a physical example where TQCP can be implemented concretely.

IV. TOPOLOGICAL PROPERTIES OF THE COOPER PAIR PUMP

One of the simplest implementation for a CPP using a superconducting circuit is represented in Fig. 5. Phase biasing is achieved by closing the CPP on a small inductance L, threaded by a magnetic flux Φ. Its magnetic contribution to the energy is $\frac{1}{2L}(\hat{\phi}-\varphi)^2$, where $\hat{\phi}$ is the phase difference across L. For small L, it has a deep minimum at $\varphi=2\pi\frac{\Phi}{\Phi_0}$: This inductance and the CPP series capacitance C_s form an harmonic oscillator whose frequency $(2\pi\sqrt{LC_s})^{-1}$ exceeds all other energies, effectively blocking the quantum variable $\hat{\phi}$ at the value φ (the center of the ground state wave function). φ is then a parameter tunable by the magnetic flux Φ.

The three Josephson junctions, with small capacitances, define two superconducting islands with sufficient large electrostatic energies to limit charge fluctuations through the

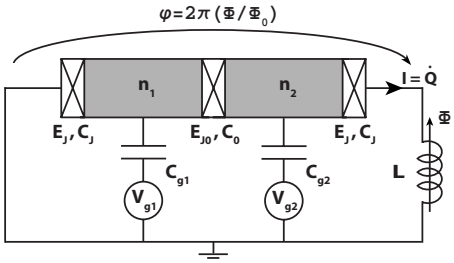

FIG. 5. The circuit is made of a Cooper pair pump closed on a small inductance L, threaded by a magnetic flux Φ. The charge on islands 1 and 2 can be tuned by two gate voltages V_{g1} and V_{g2}. The inductance is used to bias the phase across the CPP, $\varphi=2\pi\Phi/\Phi_0$.

junctions. Let n_i be the excess number of Cooper pairs (with respect to charge neutrality) on island i. The electrostatic energies of each island can be tuned independently using a gate voltage V_{g_i} through the gate capacitances C_{g_i}. The induced charge polarization on the island i is $n_{g_i}=C_{g_i}V_{g_i}/(2e)$ in units of $2e$. For convenience, we use the total charge $n_s=n_1+n_2$ on the double island and the charge asymmetry $n_d=n_1-n_2$ between them as the natural basis of charge states $\{|n_s,n_d\rangle\}$. Taking the two external junctions with the same Josephson energy E_J and capacitance C_J, and (E_{J0},C_0) for the central junction Josephson energy and capacitance, the charging energy of the CPP reads

$$\hat{\mathcal{H}}_C=E_C[(\hat{n}_s-n_{gs})^2+\kappa_0(\hat{n}_d-n_{gd})^2], \tag{46}$$

where $E_C=\frac{(2e)^2}{4C_J}$ is the Coulomb energy, $n_{gs}=n_{g_1}+n_{g_2}$, $n_{gd}=n_{g_1}-n_{g_2}$, and $\kappa_0=\frac{C_J}{2C_0+C_J}$ is a capacitance ratio (of order $\frac{1}{3}$). In addition to the phase bias φ, the induced charges n_{gs} and n_{gd} are tunable parameters of the Hamiltonian: The parameter space $\mathbb{P}$ is here three dimensional, and a point $\mathbf{R}$ in $\mathbb{P}$ is specified by its coordinates (n_{gs},n_{gd},φ). One easily checks that the charge state $|n_s,n_d\rangle$ is the ground state that minimizes the parabolas in $\hat{\mathcal{H}}_C$ [Eq. (46)] inside the hexagonal area $h_{(n_s,n_d)}$ centered at the point $(n_{gs}=n_s,\ n_{gd}=n_d)$ in the n_{gs}-n_{gd} plane (Fig. 6). On the line boundaries between hexagons, two electrostatic states have the same energies while the vertices are points of triple degeneracies. This hexagonal lattice of triple degeneracies has two points in its unit cell, chosen here as $\{T_1\}=\left(n_{gs}=\frac{1+\kappa_0}{2},n_{gd}=0\right)$ and $\{T_2\}=\left(n_{gs}=\frac{1-\kappa_0}{2},n_{gd}=1\right)$. The Josephson tunneling, which "translates" Cooper pairs across the junctions, can be expressed in terms of the variables conjugate to the total charge $\hat{n}_s$ and charge asymmetry $\hat{n}_d$, $\hat{\Theta}_s$ and $\hat{\Theta}_d$, which are the generators of charge translations,

$$\hat{\mathcal{H}}_J=-2E_J\cos\hat{\Theta}_s\cos(\hat{\Theta}_d-\kappa_J\varphi)-E_{J0}\cos(2\hat{\Theta}_d+\kappa_0\varphi), \tag{47}$$

where $\kappa_J=\frac{C_0}{2C_0+C_J}=\frac{1-\kappa_0}{2}$ is the other capacitance ratio (also of order $\frac{1}{3}$). Since $\hat{\mathcal{H}}_J$ delocalizes Cooper pairs, the charge states are no longer eigenstates of the full Hamiltonian $\hat{\mathcal{H}}=\hat{\mathcal{H}}_C+\mathcal{H}_J$, and the degeneracies along the boundaries of the hon-

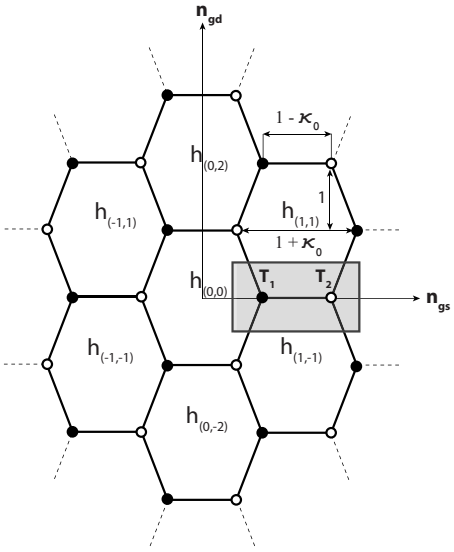

FIG. 6. Stability diagram for the charging Hamiltonian [Eq. (46)] in the n_{gs}-n_{gd} plane. The charging energy is minimized inside the hexagonal areas $h_{(n_s,n_d)}$ shown. The boundaries between hexagons are lines of degeneracies between charge states, while the vertices are points of triple degeneracies. The two vertices T_1 and T_2 form the unit cell for this hexagonal lattice. The coordinates of T_1 are $\left(\frac{1+\kappa_0}{2},0\right)$. Also shown are the topological charges of the lattice of degeneracies in the plane $\varphi=\pi$ (see text).

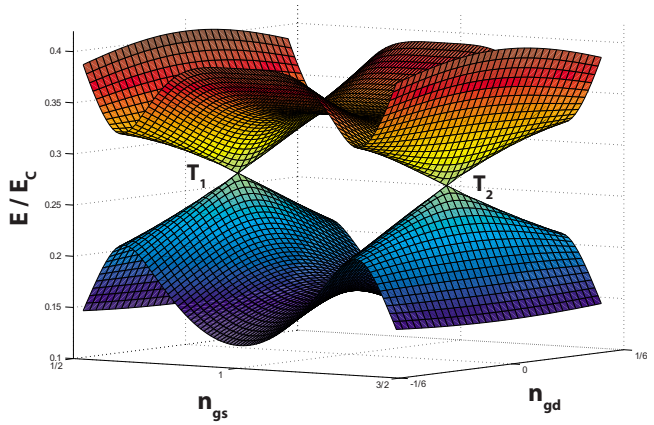

FIG. 7. (Color online) (a): The two lowest energy manifolds computed in the rectangular area of the n_{gs}-n_{gd} plane shown in Fig. 6 for the constant phase $\varphi=\pi$. In the vicinity of the isolated degeneracies $\mathbf{T}_1$ and $\mathbf{T}_2$, the energy sheets form a conical intersection, referred to as "diabolical points" (same shape as a diabolo). At these points, there are topological singularities in the bundle $\mathcal{F}^{(-)}$ [Eq. (1)].

eycomb lattice are lifted. Nevertheless, if $E_J \approx E_{J0} \leqslant E_c$, accidental isolated degeneracies persist in $\mathbb{P}$ in the vicinity of points $\mathbf{T}_1=\{T_1,\varphi=\pi\}$ and $\mathbf{T}_2=\{T_2,\pi\}$ and all their equivalents under lattice translations in $\mathbb{P}$. In the special case where $E_J=E_{J0}$ (homogenous array), the degeneracies are placed at $\mathbf{T}_1$ and $\mathbf{T}_2$, and shift along the n_{gs} axis for asymmetric arrays. As an illustration, the energy manifolds for the two lowest levels $|\pm\rangle$, represented in Fig. 7, show the two conical intersections in the points $\mathbf{T}_1$ and $\mathbf{T}_2$ in $\mathbb{P}$ for $E_J=E_{J0}$. Symmetries of the total Hamiltonian are most explicit after the unitary transformation generated by $U(\varphi)=e^{-i\kappa_J\varphi\hat{n}_d}$, which leaves the charging Hamiltonian unchanged and shifts $\hat{\mathcal{H}}_J$ into

$$\tilde{\mathcal{H}}_J = U(\varphi)\hat{\mathcal{H}}_J U^{\dagger}(\varphi) = -2E_J \cos\hat{\Theta}_s \cos\hat{\Theta}_d - E_{J0}\cos(2\hat{\Theta}_d+\varphi). \tag{48}$$

In this representation, the phase bias appears across the central junction instead of being distributed across the three junctions according to the electrostatic voltage drop. The mirror symmetry $n_{gs}\to -n_{gs}$ keeps the physics unchanged while $(\hat{n}_s,\hat{\theta}_s)\to(-\hat{n}_s,-\hat{\theta}_s)$. When the phase φ is equal to 0 or π, the Hamiltonian is real and also invariant under a second mirror symmetry $n_{gd}\to -n_{gd}$, while $(\hat{n}_d,\hat{\Theta}_d)\to(-\hat{n}_d,-\hat{\Theta}_d)$. The integer translations on the honeycomb lattice $(n_{gs},n_{gd})\to(n_{gs}+n_{s0},n_{gd}+n_{d0})$ induced by the translation operator $e^{-i(n_{s0}\hat{\Theta}_s+n_{d0}\hat{\Theta}_d)}$ leads to different numbers of Cooper pairs on the island (n_s-n_{s0},n_d-n_{d0}). These states are equivalent but physically distinguishable. Similarly, the mirror symmetry $n_{gs}\to n_{s0}-n_{gs}$ while $(\hat{n}_s,\hat{\Theta}_s)\to(n_{s0}-\hat{n}_s,-\hat{\Theta}_s)$ leaves the physics unchanged. This mirror symmetry maps the degeneracy points (or their lattice equivalents) $\mathbf{T}_1$ and $\mathbf{T}_e$ into each other. Finally, the Hamiltonian is 2π periodic in φ, and phases differing by multiple of 2π lead to identical physical states: φ plays the same role here as the ϑ^2 variable in the preceding section.

In the same fashion as in Sec. II, let us construct explicitly the two-level approximation of $\hat{\mathcal{H}}$ in the vicinity of the degeneracy point $\mathbf{T}_1$. Since circuit asymmetries do not affect the topology of the eigenvector bundle, it is simpler to take symmetric junctions $E_J=E_{J0}$ and assume that the ratio $\beta=\frac{E_J}{2E_C}$ between Josephson and charging energies remains small. Writing the small deviations from the triple point $\mathbf{T}_1$ as $\sigma=n_{gs}-\frac{2}{3}$, $\delta=n_{gd}$, $\psi=\varphi-\pi$, the projection of the Hamiltonian $\hat{\mathcal{H}}$ on the basis of charge states $\{|0,0\rangle',|1,1\rangle',|1,-1\rangle'\}$, $(|n_s,n_d\rangle'=U(\varphi)|n_s,n_d\rangle)$, is represented by the matrix

$$\hat{\mathcal{H}} = E_C\begin{pmatrix} \frac{4\sigma}{3} & -\beta & -\beta \\ -\beta & -2\frac{(\sigma+\delta)}{3} & \beta(1-i\psi) \\ -\beta & \beta(1+i\psi) & -2\frac{(\sigma-\delta)}{3} \end{pmatrix} \tag{49}$$

to first order in the deviation $\delta\mathbf{R}=(\sigma,\delta,\psi)$. At $\mathbf{T}_1$ $(\sigma=\delta=\psi=0)$, the two lowest eigenstates,

$$|+\rangle = \frac{1}{\sqrt{3}}\left(|0,0\rangle' - \frac{\sqrt{3}-1}{2}|1,1\rangle' + \frac{\sqrt{3}+1}{2}|1,-1\rangle'\right),$$

$$|-\rangle = \frac{1}{\sqrt{3}}\left(|0,0\rangle' + \frac{\sqrt{3}+1}{2}|1,1\rangle' - \frac{\sqrt{3}-1}{2}|1,-1\rangle'\right),$$

are degenerate with energy $-\frac{E_J}{2}$ (ground states), and the first excited state,

$$|e(\mathbf{T}_1)\rangle = \frac{1}{\sqrt{3}}(|0,0\rangle' - |1,1\rangle' - |1,-1\rangle'), \tag{50}$$

has E_J for an eigenvalue. As discussed in Sec. II, an isotropic spin representation of the Hamiltonian in the $|\pm\rangle$ subspace requires a deformation of the parameter space $\mathbb{P}$ represented by the matrix

$$\hat{C} = \begin{pmatrix} \frac{4}{3}E_C & 0 & 0 \\ 0 & 0 & -\frac{1}{\sqrt{3}}E_J \\ 0 & \frac{4}{3\sqrt{3}}E_C & 0 \end{pmatrix}, \tag{51}$$

which amounts here to a symmetry (the flips of the δ and ψ axes changes the space orientation) and a linear deformation. This transformation specifies the effective magnetic field ($\mathbf{b}=\hat{C}\delta\mathbf{R}$), $b^x=\frac{4}{3}E_C\sigma$, $b^y=-\frac{1}{\sqrt{3}}E_J\psi$, and $b^z=\frac{4E_C}{3\sqrt{3}}\delta$, such that the projection of the Hamiltonian on the $|\pm\rangle$ degenerate subspace reduces to a spin-$\frac{1}{2}$ Hamiltonian

$$\hat{\mathcal{H}}_{\pm(\mathbf{T}_1)} = \frac{1}{2}\begin{pmatrix} b^z & b^x - ib^y \\ b^x + ib^y & -b^z \end{pmatrix} = \frac{1}{2}\boldsymbol{\sigma}\cdot\mathbf{b}(\mathbf{R}). \tag{52}$$

The two lowest levels have a conical intersection at the degeneracy point $\mathbf{T}_1$,

$$E_\pm(\mathbf{b}) = \pm\frac{|\mathbf{b}|}{2}. \tag{53}$$

Following the discussion in Sec. II, the topological charge in the spin representation and in the original parameter space are identical up to the sign of the determinant of $\hat{C}$, which is positive. Hence, the topological charge of the ground state is $q^{(0)}(\mathbf{T}_1)=+1$ and -1 for the first excited band. Using the same arguments, the topological charge at the degeneracy $\mathbf{T}_2$ is $q^{(0)}(\mathbf{T}_2)=-1$. Similarly, all degeneracies obtained by lattice translation from $\mathbf{T}_1$ ($\mathbf{T}_2$) have a topological charge of +1 (−1) for the ground state. As mentioned in Sec. II, the transformation properties of the eigenstates bundle under mirror, and time-reversal symmetries allow us to detect the presence of a degeneracy locally (in the spin-$\frac{1}{2}$ representation). Here, the $|\pm\rangle$ states map into each other, and each eigenvector bundle is not preserved separately by these transformations. When E_{J0} deviates from E_J, the degeneracies move continuously away from $\mathbf{T}_1$ and $\mathbf{T}_2$. Using the same 3×3 matrix representation for $\hat{\mathcal{H}}$, the degeneracies slide along the n_{gs} axis in the vicinity of $\mathbf{T}_1$ and $\mathbf{T}_2$ as

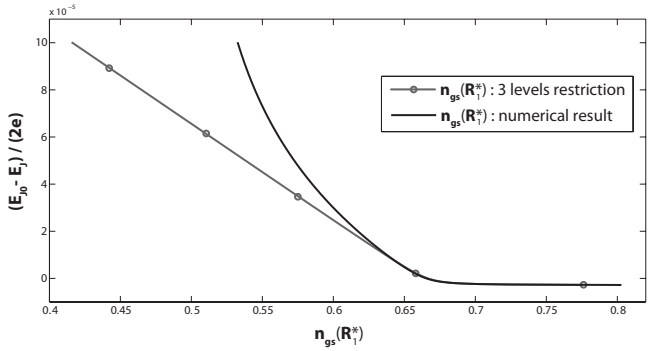

FIG. 8. Comparison of position of the degeneracy point $\mathbf{R}_1^*$ between the analytic model described in the text and the exact numerical result.

$$\mathbf{R}^*_{1,2} = \left(n_{gs}(\mathbf{T}_1) \mp \frac{1}{4E_C}\left[E_{J0} - \frac{E_J^2}{E_{J0}}\right], 0, \pi\right) \tag{54}$$

for small deviations $|E_{J0}-E_J|$. In this shift, the degeneracies keep their topological charge, $q^{(0)}(\mathbf{R}_i^*)=q^{(0)}(\mathbf{T}_i)$. In Fig. 8, the analytic and exact positions of the degeneracy points are compared: The agreement deviates rapidly as one moves away from $\mathbf{T}_1$.

The presence of degeneracies in the lowest band of the CPP allows us to quantize the pumped current opening accurate application for metrology, which is the topic of the next section.

V. QUANTIZATION IN THE COOPER PAIR PUMP

The idea of using single electron pumps[23] as current standard dates from the early 1990's. The original circuits that use normal islands separated by a tunnel junction were biased by a small dc voltage V_B. If the two gate voltages are driven in quadrature, the systems undergo a circular cycle centered around point $\mathbf{T}_1$. The electrostatic ground state changes cyclically ($|0,0\rangle\rightarrow|1,-1\rangle\rightarrow|1,1\rangle\rightarrow|0,0\rangle$) as one crosses one of the three degeneracy lines intersecting at T_1. After one cycle, a single charge is transferred through the electron pump. If the cycles are sufficiently slow, the charge relaxation (e.g., $|0,0\rangle\rightarrow|1,-1\rangle$) is inelastic but has sufficient time to complete. Since the process is stochastic, errors occur and limit the accuracies of normal electron pumps. Also, the time scale for charge relaxation is typically of order $\tau=(R_TC)^{-1}$, where R_T is the tunneling resistance. For realistic circuits, τ rarely exceeds 10^{-6} s, and pumped currents do not exceed a few picoampere.

This is one of the motivations for studying CPPs[24–26] to circumvent the stochasticity of normal electron devices. Here, we show that the charge transferred can be quantized topologically by using controlled paths in parameter space (TQCP). The CPP's circuit delivers a current I that is equal to the charge transferred Q per unit of time: $I=\dot{Q}$ (see Fig. 5). Let us return to Eqs. (46) and (47) and consider that $\hat{\varphi}$ is still a quantum degree of freedom conjugated to a charge operator $\hat{q}$, i.e., $[\hat{q},\hat{\varphi}]=i$. The time evolution of the mean value of $\hat{q}$ is $\frac{d\langle\hat{q}\rangle}{dt}=-\frac{i}{\hbar}\langle[\hat{q},\hat{\mathcal{H}}]\rangle$ and is equal to $\frac{1}{\hbar}\langle\partial_{\hat{\varphi}}\hat{\mathcal{H}}\rangle$. Since the small

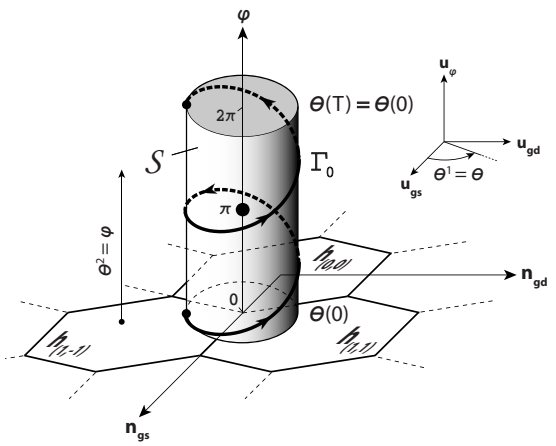

FIG. 9. A helical closed path Γ_0 in $\mathbb{P}$ on the surface of a cylinder enclosing the degeneracy $\mathbf{T}_1$. Since φ is cyclic, the surface $\mathcal{S}$ is a two-dimensional torus and Γ_0 is closed for integer frequency ratio $p=\nu_\theta/\nu_\varphi$ (here 2).

inductance blocks the quantum fluctuation in $\hat{\varphi}$, it can be taken as classic and the pumped current is

$$I=\dot{Q}=\frac{2e}{\hbar}\langle\partial_\varphi\hat{\mathcal{H}}\rangle. \tag{55}$$

Since φ and ϑ^2 have the same 2π periodicity, $\frac{\hbar}{2e}I$ has the exact expression [Eq. (21)] as required for the TQCP procedure discussed in Sec. III. Consider now the cylinder $\mathcal{S}$ in parameter space represented in Fig. 9, whose axis lies in the φ direction. Its section in the n_{gs}-n_{gd} plane has a radius ρ of order $\frac{1-\kappa_0}{2}\simeq\frac{1}{3}$, and its height on the φ axis is 2π. Since the end faces $\varphi=0$ and $\varphi=2\pi$ are physically equivalent, this cylinder $\mathcal{S}$ is a closed surface and has the topology of a torus $\mathbb{T}^2$. A point on $\mathcal{S}$ is specified by two angles ϑ^1, the angle in the n_{gs}-n_{gd} plane and the phase $\varphi\equiv\vartheta^2$. The cylinder's radius ρ is chosen so as to include only one degeneracy $\mathbf{T}_1$. It has the same Chern index as any other surface, which includes $\mathbf{T}_1: c_1^{(0)}(\mathcal{S})=q^{(0)}(\mathbf{T}_1)=+1$ with respect to the ground level. By deformation, the cylinder offers the advantage to contain the same helical paths [Eq. (25)] as the one on the torus used in Sec. III. TQCP can therefore be used exactly in the same fashion for the topological charge, which is quantized as

$$\langle Q\rangle=\frac{2e}{\hbar}p\hbar c_1^{(0)}(\mathcal{S})=2ep \tag{56}$$

when averaged over the initial phase λ of the helix [defined in Eq. (25)], making p turn around T_1.

Since Eq. (41) gives the incremental charge transferred, this quantity can be monitored continuously as one moves along the helical open path using Eq. (39). The Josephson couplings E_J and $E_{J0}\simeq E_J$ lift the degeneracies between the charged states along the three boundary lines of the hexagons intersecting at T_1, which become saddle lines [see Figs. 6 and 10(b) for the saddle lines of the ground state]. The splitting between the ground state $|-\rangle$ and the first excited state $|+\rangle$ is smallest along the saddle lines and is of the order of E_J. As one moves on the helical path, each saddle line is crossed once per turn around T_1. Since the accuracy of the CPP hinges on the ability to move adiabatically in the ground state manifold, the Landau-Zener transition $|-\rangle\rightarrow|+\rangle$ when crossing a saddle line is a concern. The transition probability $P_{L-Z}\simeq e^{-\left(\frac{3\pi}{2}\right)^2\frac{E_J}{E_C}\frac{E_J}{h\nu_\theta}}$ depends on the ratios $\frac{E_J}{E_C}$ and $\frac{E_J}{h\nu_\theta}$, which cannot be too small. On the other hand, when the ratio $\frac{E_J}{E_C}$ is too large, the dynamical contribution to the charge transferred is more difficult to average out and the accuracy of the device deteriorates. This is the tradeoff when optimizing the CPP: A large E_J reduces Landau-Zener tunneling and allows for a higher frequency of operation, but the Josephson current can be most easily driven to zero at small E_J. To avoid single electron effects, the charging energy E_C has to be

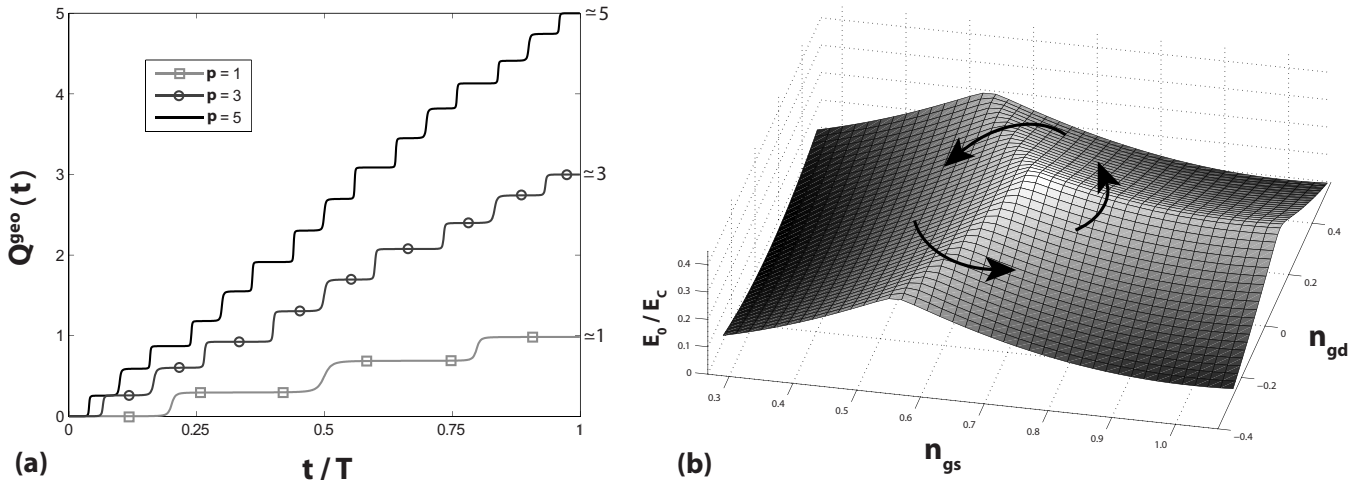

FIG. 10. (a) Geometric transferred charge Q^{geo} as a function of t for the helical paths defined in Eq. (25) and $p=1,3,5$. (b) Each time the path crosses one of the three saddle lines (here plotted for $\varphi=\pi$), approximately a third of one charge unit is geometrically transferred. The computation was done using a radius $\rho=0.3$, $\lambda=0$, and the Josephson couplings and charging energies of a real device: $E_J=6$ μeV, $E_{J0}=8.6$ μeV, $C_J=0.78$ fF, and $C_0=0.69$ fF.

smaller than the superconducting gap (0.2 meV for aluminum). This sets the overall energy scale and most of the parameters: Typically, values for $E_C \approx 0.1$ meV, $E_J \approx 0.05E_C$, and $\nu_\theta \approx 100$ MHz offer a good optimization of the CPP. The parameters of the helical path are the radius ρ and the number of turns p in a period $T_\varphi = \frac{2\pi}{\nu_\varphi}$. For the optimal radius $\rho = \frac{1-\kappa_0}{2} \approx \frac{1}{3}$, the path intersects the line between T_1 and T_2 in the middle. A smaller radius is equivalent to reducing E_C.

Now that the parameters are known, the charge transferred can be followed as one moves along the helical paths defined in Eq. (25). p is here the number of turns around T_1 in a period T_φ. Integrating the instantaneous transferred charge [Eq. (41)] for the ground state $|-\rangle$ yields the time dependence of Q^{geo},

$$Q^{\text{geo}}(t) = \int_0^t \delta Q^{\text{geo}}(t'), \tag{57}$$

which is plotted as a function of time in Fig. 10 using the parameters of a real device $\left(\frac{E_J}{E_C} \approx 0.05\right)$ and Eq. (41). For small $\frac{E_J}{E_C}$ ratios, the charge is transferred in three distinct steps, corresponding to the transfer of a Cooper pair through each junction, which occurs when crossing the three saddle lines. Two steps are of height $\simeq \kappa_J$ (external junctions) while one is of height $\simeq \kappa_0$, yielding a total transferred charge $\simeq 2\kappa_J + \kappa_0 = 1$ per turn (in units of $2e$), as illustrated in Fig. 10 where this quantity is plotted for different numbers of turns (p). The steps rounding become more pronounced as E_J increases, and their size more sensitive to the initial phase value $\varphi(0) = \lambda$.

Clearly, the charge transferred value $\simeq 2e$ is due to the presence of the degeneracy with topological charge +1. We now verify that quantization accuracy improves as p increases, a fundamental feature of TQCP,

$$Q(\Gamma_\lambda) \underset{p\to\infty}{\to} 2ep. \tag{58}$$

The geometric and dynamical charges transferred in the CPP ground state can be followed as a function of the initial phase λ. For optimal values of the parameters ($E_C \approx 100$ μeV and $E_J \approx 3$ μeV), the errors computed are small. In the simulation, it is useful to amplify their effects by choosing the most unfavorable parameters. Using a perturbative analysis, the dynamical contributions to the pumped charge are of order $Q^{\text{dyn}} \approx \frac{T_\varphi}{\hbar}\frac{E_J^3}{E_C^2}$ in units of $2e$.[27] Similarly, the deviations of the geometrical pumped charge from its quantized value scale as $\frac{E_J^2}{E_C^2}$. Hence, larger values of E_J/E_C increase errors. In Fig. 11, the geometrical and the dynamical charge transferred are plotted for a ratio $E_J/E_C = 0.5$, an order of magnitude larger than the optimal values. On this figure, the charges are computed using helical paths around $\mathbf{T}_1$ with different numbers of windings in a period T_φ. The geometrical charge oscillates as a function of λ around the quantized value with an amplitude that decreases rapidly with the number of windings p. This rate depends mostly on E_J/E_C and on the distance between each winding relative to the distance to the degeneracy

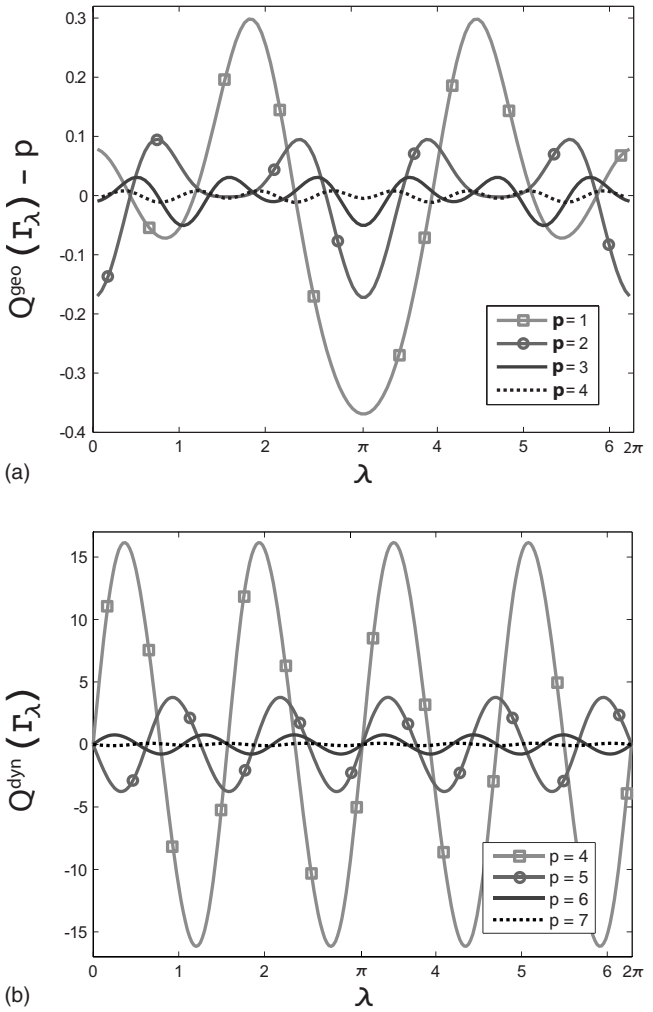

FIG. 11. (a) Plot of the geometric charge Q^{geo} as a function of λ for helices with different numbers (1–4) of windings. (b) Same plot for the dynamical charge Q^{dyn} as a function of λ using four to seven windings. Parameters: $\rho = 0.3$, $E_J = E_{J0} = 60$ μeV, and $E_C = 114$ μeV.

$\mathbf{T}_1$. This is the main reason for keeping the helix radius close to its optimal value $\left(\frac{1-\kappa_0}{2}\right)$.

For parameters closer to their optimal value, this decrease can be expressed in terms of ξ, the root mean square amplitude of the oscillations. This quantity is tabulated as in Table I using $E_J/E_C = 0.05$. Above a few windings, the quantization accuracy is very high. If low frequencies phase jitters in $\delta\varphi$

TABLE I. Mean root square deviations of the different contributions to the transferred charge as a function of p. Numeric values: $\rho = 0.3$, $\lambda = 0$, $E_J = 60$ μeV, and $E_J/E_C \approx 0.5$.

p	ξ_{geo}	ξ_{dyn}	ξ_{tot}
1	8.7×10^{-3}	5.4	5.4
2	2.8×10^{-3}	4.2×10^{-3}	5.0×10^{-3}
3	3.8×10^{-4}	1.3×10^{-3}	1.3×10^{-3}
4	3.9×10^{-5}	9.1×10^{-5}	9.9×10^{-5}
5	4.6×10^{-6}	5.5×10^{-6}	7.2×10^{-6}

are present, the error in the pumped charge will be of the order of $\xi_{\mathrm{geo}}(p)\frac{\delta\varphi}{2\pi}$, which is below 10^{-8} for $p \geqslant 5$.

The average dynamical charge transferred over a period converges also toward zero when p is sufficiently large, provided that the ratio of $\frac{E_J}{E_C}$ is not too large (say, below 0.05). In the absence of noise, the periodicity in φ guarantee that it averages out to zero. In the presence of a phase noise $\delta\varphi$, the cancellation becomes approximate with an error of the order of $\xi_{\mathrm{geo}}(p) \sim \frac{\delta\varphi}{2\pi}$.

It is not possible to reduce the ratio E_J/E_C arbitrarily to improve the accuracy because the gap at the saddle points ($\propto E_J$) decreases and the Laudau-Zener tunneling turn on the transition to the first excited manifold. This introduces the largest source of errors because the Chern indices of the two lowest eigenvector bundles are opposite, an issue which is addressed in the concluding section.

VI. ADIABATIC COMPUTING

In the vicinity of a triple point T_1, the two lowest states $|\pm(\mathbf{R})\rangle$ form a qubit. In this region of $\mathbb{P}$, the next level $|e(\mathbf{R})\rangle$ lies at an energy of the order of $\frac{3}{2}E_J$ above the $|\pm\rangle$ doublet, significantly larger than the doublet splitting. One-qubit operations on this doublet can be implemented using different schemes.

The simplest one consists in applying microwave pulses to the CPP gates at the frequency splitting between the $|\pm(\mathbf{R})\rangle$ states. The point $\mathbf{R}$ may be chosen at one of the magical points along the saddle lines of the hexagons where the system is to first order insensitive to gate charge and phase fluctuations.[2] However, there are simpler circuits where such operations have been demonstrated and the CPP is more interesting to implement quantum computation using adiabatic cycles. Duan *et al.*[28] have shown how geometric gates could be implemented on a degenerate two-level system using resonant transitions between this $|\pm\rangle$ doublet and an excited level $|e\rangle$, provided that it is also coupled to an auxiliary level $|a\rangle$. In the CPP, $|a\rangle$ could, in principle, be a higher lying charge state, but this solution is not as convenient as for atomic systems. We prefer to do without the $|a\rangle$ state. In this case, the dynamical contribution associated with the Rabi frequency cannot be eliminated altogether. As long as this phase shift can be tuned to a multiple of π, a geometric gate can be implemented.

The CPP is biased at degeneracy ($\mathbf{T}_1$), and microwave voltages tuned at the $|e\rangle - |\pm\rangle$ frequency splitting are applied to *both* gates. When going to a frame rotating at the same frequency, the coupling to the $|e\rangle$ state becomes time independent

$$\hat{\mathcal{H}}_{\mathrm{mw}}(t) = \hbar\Omega\left(\cos\frac{\zeta}{2}|e\rangle\langle -| + \sin\frac{\zeta}{2}e^{i\chi}|e\rangle\langle +| + \mathrm{H.c.}\right), \tag{59}$$

where Ω is the main Rabi frequency, and the angle ζ controls the relative strength of the couplings of the $|+\rangle$ and $|-\rangle$ to the $|e\rangle$ state, while χ is their relative phase. These three quantities can be adjusted by tuning the amplitude and the phase of the microwave voltages applied to the CPP gates. Here, 2π phase cycles in χ are sufficient to generate the gate operations. In the rotating frame, one of the sates is stationary, while the other two oscillate at $\pm\Omega$. Adjusting the period of operation T to eliminate the dynamical phase shift ($e^{i\Omega T} = \pm 1$), a 2π cycle in χ generates the operation

$$G(\zeta, 2\pi) = \begin{pmatrix} \cos(\pi\cos\zeta)\cos\zeta + i\sin(\pi\cos\zeta) & -\cos(\pi\cos\zeta)\sin\zeta \\ \cos(\pi\cos\zeta)\sin\zeta & \cos(\pi\cos\zeta)\cos\zeta - i\sin(\pi\cos\zeta) \end{pmatrix}, \tag{60}$$

which covers all the one-qubit gate operation.

Two-qubit geometrical gates can also be considered by coupling two Cooper pair pumps together. One way this may be achieved is to close the two pumps on the same inductance L: The current pumped in both devices add up in L, shifting the phase φ by an amount of order LI_j, where I_j is the current through the jth CPP.

In practice, adiabatic computing[29] faces a number of difficulties. Even for one-qubit operations, three or more states have to be degenerate. However, any low frequency flux or charge noise moves the area in parameter space where the degeneracy occurs and the shifts in parameters rotate the eigenvectors rapidly. While this has little impact for topological quantization, this deteriorates the performance of geometrical gates. The accuracy with which parameters are to be controlled is also considerably higher than for usual quantum gates. These are some of the reasons why geometrical gates have not yet been demonstrated.

VII. CONCLUSIONS

Most limitations for adiabatic computing are irrelevant to topological quantization, which is robust against most perturbations. For a CPP, charge or phase noise is considered slow when most of its spectrum is below the frequency of operation of the pump ν_θ (100 MHz is a realistic number). Such noise source adds a random component to the controlled voltage or the magnetic flux, and the path in $\mathbb{P}$ no longer generates a cylinder but a more irregular surface. As far as the geometrical charge is concerned, this has almost no effect, as long as the resulting surface still encloses the topological point $\mathbf{T}_1$. Similarly, if the junction capacitances or

Josephson couplings fluctuate in time, the position of the point $\mathbf{T}_1$ fluctuates in $\mathbb{P}$, and this has little effect as long as this shift is small compared to the cylinder's radius. In the presence of low frequency noise, dynamical contributions no longer cancel exactly. On the other hand, the errors are random and can be averaged using long integration times.

If charge or phase noise has frequency components at the splitting between the two lowest states $|\pm(\mathbf{R})\rangle$ or if the Landau-Zener transition occurs at one of the three saddle point crossings (see Sec. V for a discussion), the system will spend a fraction of the time in the first excited state. Since the Chern index of the $|+\rangle$ state is opposite to the ground state, this will introduce an error in the pumped charge proportional to the relative time spent in the excited state. This is why high frequency noise must be thoroughly filtered and the pumped speed adjusted to quench Landau-Zener transitions.

This study of quantization by controlled path, although conducted around CPP circuits, is quite general. The necessary criteria, which have been stated in the Introduction, are now discussed in more detail

1. The adiabatic condition can only be satisfied for discrete spectra. Furthermore, adiabaticity only holds well for a quantum state if its energy splittings with other levels are sufficient.

2. The presence of isolated degeneracies between two lowest states is required. For a complex Hamiltonian, this is possible only if it depends on three continuous parameters. In quantum circuits, tunable parameters are typically gate voltages and magnetic fluxes. For Cooper pair pumps, the parameters are two gate charges and a phase (CPP) or two phases and a charge (the sluice pump[27]). The parameters are used to generate controlled paths in the three-dimensional parameter space $\mathbb{P}$. Additional parameters are useful for adiabatic computations (Sec. V). There are two recipes to locate the degeneracies. The first one hinges on their topological signature on Berry's phase (π). As argued by Stone,[30] one can divide the parameter space $\mathbb{P}$ in small volumes around which Berry's phase is computed. If a single degeneracy exists inside the loop, Berry's phase picks it up. Another method is to detect the vorticity of the eigenvector bundle in the vicinity of a degeneracy (see Secs. II and IV): In this case, the "mirror symmetry" and "T symmetry" are broken for the ground state; i.e., they flip the eigenvector bundles intersecting at the degeneracy (Kramers symmetry).

3. Only observables proportional to the partial derivative of the Hamiltonian $\hat{\mathcal{H}}$ with respect to one of the tunable parameters ϑ^2 (φ for the CPP) can be quantized using TQCP. In this case, its averaged expectation value over a closed surface $\mathcal{S}$ around a degeneracy is proportional to the Chern index of this surface. When the variable is periodic, we may choose this surface with the topology of a torus. A path sweeping this surface or covering it densely is the controlled path expressing the quantization.

Although topological quantization is quite robust, transitions to the first excited state (induced by fluctuations or Landau-Zener processes) are problematic because the Chern indices of the two lowest levels have opposite signs.

The above criteria only concern geometrical contributions. However, the dynamical evolution of the observable may also contribute. An accurate quantization is possible if they can be eliminated through symmetries or other schemes. This depends to some extent on the physical problem at hand. For quantum circuits, the following condition is sufficient to average them out.

1. The Hamiltonian and the surface $\mathcal{S}$ are periodic in the parameter φ, or have some symmetry with respect to φ, such that the dynamical contribution averages to zero.

The value of the topological quantization is its strong robustness to adiabatic parameter fluctuations, the Chern index of the surface enclosing the degeneracy being the quantum number of the quantity of interest. For a Cooper pump, the magnitude of the current generated

$$I = 2ec_1^{(0)}(\mathbf{T_i})\nu_\theta \tag{61}$$

is of the order of 30 pA for realistic values of the parameters.

One of the potential applications for a Cooper pair pump is as an accurate current source[31] to close the metrology triangle,[32] relating frequency to voltage through the Josephson effect, voltage to current through the quantum Hall effect, and frequency to current through topological pumping. It is interesting to note that all these effects are the result of topological quantization.[8–11] In order to be useful in this context, where the pumped current feeds a Hall bar, a higher current is needed (100 nA or higher[33]). Large gain amplification schemes are being designed to fulfill this condition. Another method for a current-frequency conversion relies on Bloch oscillation.[34] This method has been recently demonstrated by the quantronium group.[35] This method, also based on a topological quantization (Thouless pumping[10]), also appears to be quite promising.

To conclude, we have stressed the importance of topological quantization in superconducting circuits. We showed how closed paths can be chosen in parameter space to generate a surface on which the charge Q is quantized by a Chern index. We have also shown how the charge transferred on any path could be obtained, giving also a local picture that cannot be derived from the usual global geometrical picture. Finally, the technique developed around superconducting circuits is quite general and can be applied to any problems in which the criteria listed in the Introduction and Conclusion are satisfied.

ACKNOWLEDGMENTS

R.L. acknowledges financial support from the Rhône-Alpes region (Micro-Nano cluster). We are quite grateful to Frédéric Faure for many enlightening discussions.

[1] Y. Nakamura, Yu. A. Pashkin, and J. S. Tsai, Nature (London) **398**, 786 (1999).
[2] D. Vion, A. Aassime, A. Cottet, P. Joyez, H. Pothier, C. Urbina, D. Esteve, and M. H. Devoret, Science **296**, 886 (2002).
[3] G. Herzberg and H. C. Longuet-Higgins, Discuss. Faraday Soc. **35**, 77 (1963).
[4] F. Faure and B. Zhilinskii, Phys. Rev. Lett. **85**, 960 (2000).
[5] B. I. Zhilinskii, Phys. Rep. **341**, 85 (2001).
[6] W. Wernsdorfer and R. Sessoli, Science **284**, 133 (1999); W. Wernsdorfer, N. E. Chakov, and G. Christou, Phys. Rev. Lett. **95**, 037203 (2005).
[7] P. Bruno, Phys. Rev. Lett. **96**, 117208 (2006).
[8] D. J. Thouless, M. Kohmoto, M. P. Nightingale, and M. den Nijs, Phys. Rev. Lett. **49**, 405 (1982).
[9] M. Kohmoto, Ann. Phys. **160**, 343 (1985).
[10] D. J. Thouless, Phys. Rev. B **27**, 6083 (1983).
[11] J. Goryo and M. Kohmoto, arXiv:cond-mat/0606758, Mod. Phys. Lett. B (to be published).
[12] M. V. Berry, Proc. R. Soc. London, Ser. A **392**, 45 (1984).
[13] B. Simon, Phys. Rev. Lett. **51**, 2167 (1983).
[14] J. von Neumann and E. P. Wigner, Phys. Z. **30**, 467 (1929).
[15] T. T. Wu and C. N. Yang, Nucl. Phys. B **107**, 365 (1976).
[16] L. Landau, Phys. Z. Sowjetunion **2**, 46 (1932); C. Zener, Proc. R. Soc. London, Ser. A **137**, 696 (1932); E. C. G. Stueckelberg, Helv. Phys. Acta **5**, 369 (1932).
[17] L. I. Schiff, *Quantum Mechanics*, 3rd ed. (McGraw-Hill, New York, 1968).
[18] M. Aunola and J. J. Toppari, Phys. Rev. B **68**, 020502(R) (2003).
[19] M. Möttönen, J. P. Pekola, J. J. Vartiainen, V. Brosco, and F. W. J. Hekking, Phys. Rev. B **73**, 214523 (2006).
[20] R. D. King-Smith and D. Vanderbilt, Phys. Rev. B **47**, 1651 (1993).
[21] R. Resta, Rev. Mod. Phys. **66**, 899 (1994).
[22] V. Bargmann, J. Math. Phys. **5**, 862 (1964).
[23] P. Lafarge, P. Joyez, D. Esteve, C. Urbina, and M. H. Devoret, Nature (London) **365**, 422 (1993).
[24] A. B. Zorin, F. J. Ahlers, J. Niemeyer, T. Weimann, H. Wolf, V. A. Krupenin, and S. V. Lotkhov, Phys. Rev. B **53**, 13682 (1996).
[25] E. Bibow, P. Lafarge, and L. P. Lévy, Phys. Rev. Lett. **88**, 017003 (2001).
[26] A. O. Niskanen, J. P. Pekola, and H. Seppa, Phys. Rev. Lett. **91**, 177003 (2003).
[27] J. P. Pekola, J. J. Toppari, M. Aunola, M. T. Savolainen, and D. V. Averin, Phys. Rev. B **60**, R9931 (1999).
[28] L.-M. Duan *et al.*, Science **292**, 1695 (2001).
[29] P. Zanardi and M. Rasetti, Phys. Lett. A **264**, 94 (1999).
[30] A. J. Stone, Proc. R. Soc. London, Ser. A **351**, 141 (1976).
[31] J. J. Vartiainen, M. Möttönen, J. P. Pekola, and A. Kemppinen, Appl. Phys. Lett. **90**, 082102 (2007).
[32] F. Pikemal and G. Geneves, Metrologia **37**, 217 (2003).
[33] F. Delahaye and B. Jeckelmann, Metrologia **40**, 217 (2003).
[34] D. V. Averin, A. B. Zorin, and K. K. Likharev, Zh. Eksp. Teor. Fiz. **88**, 692 (1985).
[35] F. Nguyen, N. Boulant, G. Ithier, P. Bertet, H. Pothier, D. Vion, and D. Esteve, Phys. Rev. Lett. **99**, 187005 (2007).